

# Numerical analyses of effective dielectric constant of multiphase microporous media

Moran Wang<sup>a)</sup> and Ning Pan

*Department of Biological and Agricultural Engineering, University of California, Davis, California 951616*

(Received 25 January 2007; accepted 15 April 2007; published online 7 June 2007)

This paper provides a full numerical tool set for modeling and predicting an effective apparent dielectric constant of multiphase microporous media, which includes a multiparameter random generation-growth algorithm for generating microstructures of multiphase porous media and a lattice Boltzmann solver for the electric potential transport equations through porous structures. After being validated by the theoretical solutions for simple geometries, the present methods are used to investigate the phase distribution effects on the effective dielectric constant of multiphase microporous media, including the effects of particle size, structure anisotropy, and phase aggregation caused by wetting characteristics between phases for multiphase cases. The resultant predictions at the end agree well with the existing experimental data for both two-phase and three-phase cases. © 2007 American Institute of Physics. [DOI: 10.1063/1.2743738]

## I. INTRODUCTION

Predicting the electric properties of a medium composed of a mixture of different dielectric materials has been a challenging problem of both theoretical and practical importance.<sup>1-5</sup> These heterogeneous systems composed of two or more phases show different conductive and dielectric properties depending on not only the electric property and volume fraction of each phase but also the geometrical shapes and arrangements of the inclusions.<sup>6,7</sup> Most popular theoretical models for the dielectric constant of porous media are based on networks of parallel and series modes<sup>8-11</sup> or introducing the morphology effects of a porous structure by some empirical parameters.<sup>12-21</sup> No analytical model has been found that deal successfully with a dielectric constant of natural porous media with random phase distributions and interactions up to now.<sup>22</sup>

Owing to the rapid developments of computers and computational techniques in the past twenty years, numerical modeling methods have been increasingly used to predict an effective dielectric constant of porous media. A complete numerical determination of dielectric properties of porous media should include two aspects: acquiring and reproducing random multiphase structures in terms of computer data correctly and solving the relevant set of local electric potential transport equations efficiently.

Several methods have been proposed to generate microstructures of multiphase materials in the past decade. The random location of obstacles is the simplest one to construct an artificial porous medium when the microstructure details are negligible.<sup>7,23,24</sup> Tacher *et al.*<sup>25</sup> presented a discrete reduced distance method to generate spherical/elliptical two-phase granular porous media. Based on the work of Tacher *et al.*, Pilotti developed a grain sedimentation algorithm.<sup>26</sup> Both the methods of Tacher *et al.* and Pilotti generate porous media with random size and locations, however, neither can deal well with the interactions between grains. Therefore nei-

ther is suitable for electric transport problems which are extremely sensitive to contacts. Recently, the reconstruction process has been widely used in generating random two-phase<sup>27,28</sup> and multicomponent<sup>29,30</sup> porous materials based on the digital microtomographic information and statistical correlation functions.<sup>31</sup> This kind of reconstruction method is more suitable for nonfluidic or single-fluid systems rather than for multiple fluid systems. Mohanty<sup>32</sup> therefore generated unsaturated porous media using a Monte Carlo annealing algorithm by means of the law of lowest interfacial energy. Wang *et al.*<sup>33,34</sup> proposed a multiparameter random generation-growth method, termed as the quartet structure generation set (QSGS), to replicate randomly distributed multiphase porous media based on the cluster growth theory<sup>35</sup> and then investigated thermal properties of porous media.

Conventional partial difference equation (PDE) solvers, such as the finite difference method (FDM),<sup>36-39</sup> finite element method (FEM),<sup>40-43</sup> and boundary element method (BEM),<sup>44,45</sup> have been applied to tackle the governing equations of electric potential transports in porous media or binary mixtures. However, the structural complexities bring in two challenges when the governing equations are to be solved by conventional PDE solvers. The first is the requirement of a grid refinement for complex structures: The accuracy of a conventional numerical method is strongly dependent on the grid size so that an extra fine grid is needed whenever the transport process is complex in physics and/or in geometry. When dealing with multiphase conjugate transport problems in porous media with complex geometries, this requirement will confine the computational domain into a very limited area in practice. The second is the conjugate constraint on interfaces between different phases: For a steady electric field transport through multiphase structures, electric potential and flux continuities have to be ensured at the interfaces when solving the governing equations, thus demanding extremely high computational resources for a porous medium with innumerable interfaces in the structure. To overcome such difficulties, few methods based on stochastic-

<sup>a)</sup>Electronic mail: mmwang@ucdavis.edu

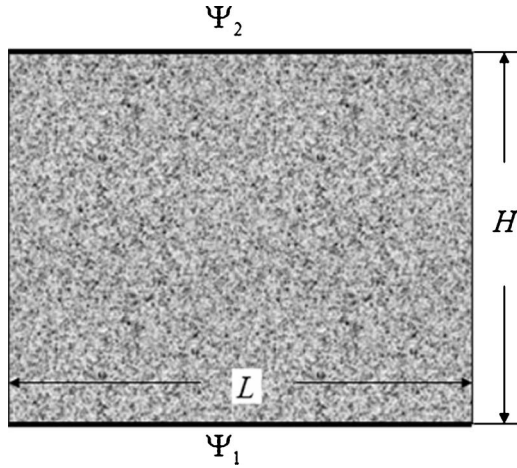


FIG. 1. A parallel plate capacitor with multiphase porous internal structure.

statistic theories have gained much attention for porous media applications recently.<sup>5,46,47</sup> For example, Yue *et al.*<sup>48,49</sup> have developed a lattice gas automata method to predict the electric transport properties in two-dimensional multiphase porous media.

The objective of the present work is to provide a full numerical tool set for modeling and predicting a frequency-independent effective dielectric constant of multiphase microporous media, including a multiparameter random generation-growth algorithm termed as QSGS for reproducing microstructures of multiphase porous media into the analysis, with further improvement in this study to emphasize the macroscopic parameter effects on the microstructures, and a lattice Boltzmann algorithm for solving the electric potential transport equations through porous structures, more efficient than any other widely used PDE solvers for complex structures, especially with the multiphase conjugate transport effect considered. The article is organized as follows. In Sec. II, we present the governing equations along with the corresponding boundary conditions, and in Sec. III we introduce the employed numerical methods, including the QSGS for generating microstructures of multiphase microporous media and the high-efficiency lattice Boltzmann algorithm. Numerical results are gathered in Sec. IV. After the numerical methods are validated by existing theoretical solutions for simple cases, the new tools are used to analyze the effects of phase distributions on the effective dielectric constant of multiphase microporous media including the influences of the grain size, the system anisotropy, and the multiphase interactions. Finally the predictions are compared with published experimental data.

## II. GOVERNING EQUATIONS

Once the effective medium theory (EMT) is applicable,<sup>50</sup> the electric potential transport in a multiphase porous medium can be governed by the Laplace equation when there are no current sources within the domain.<sup>41,42</sup> Let us consider a parallel plate capacitor with a constant potential difference as shown in Fig. 1. An uncharged porous medium fills the capacitor space  $L$  long and  $H$  high. The governing equation for electric potential transport is

$$\nabla[\varepsilon_r(r) \nabla \Psi(r)] = 0, \quad (1)$$

where  $r$  is the position,  $\varepsilon_r$  represents the local relative dielectric constant of medium, and  $\Psi$  is the local electric potential, in conjunction with the following boundary conditions:

$$\Psi|_{y=0} = \Psi_1, \quad (2)$$

$$\Psi|_{y=H} = \Psi_2. \quad (3)$$

The edge fringing effect can be eliminated by a periodic extension at the following conditions:

$$\mathbf{n} \cdot \nabla \Psi|_{x=0,L} = 0, \quad (4)$$

where  $\mathbf{n}$  denotes the unit vector normal to the surface considered. As mentioned above, there are lots of phase interfaces within such porous media. On each interface between phase  $m$  and phase  $n$ , the potential and flux are supposed to be continuous, i.e.,

$$\Psi^m = \Psi^n, \quad (5)$$

$$D^m = D^n, \quad (6)$$

where  $D$  is the electric flux,

$$D = \varepsilon_0 \varepsilon_r \mathbf{n} \cdot \nabla \Psi, \quad (7)$$

and  $\varepsilon_0$  is the dielectric constant of vacuum.

After the electric potential field is solved, the global effective dielectric constant  $\varepsilon_{\text{eff}}$  is then defined by the mean electric flux  $\langle D \rangle$  and mean potential gradient  $\langle \nabla \Psi \rangle$ ,<sup>51</sup>

$$\varepsilon_{\text{eff}} = \frac{\langle D \rangle}{\varepsilon_0 \langle \nabla \Psi \rangle}. \quad (8)$$

## III. NUMERICAL METHODS

### A. The quartet structure generation set for multiphase porous structure

Here we use our QSGS method<sup>33</sup> to generate microstructures of multiphase microporous media, whose flow chart is schemed in Fig. 2 and the algorithm is described as follows.

Before initiation, one has to determine among the different phases a nongrowing phase and the rest will be the growing ones. For generality, we call each growing phase as  $n$ th phase, where  $n=2, \dots, N$ , the total number of phases in the system. Customarily without losing generality, the discrete phases are taken as the growing phases. For example, rocks and moisture are the growing phases in unsaturated sands, whereas gas is the growing phase in polyurethane foams. Then the structure growing process follows the steps below:

- (i) Randomly locate the cores of the first growing phase in a grid system based on the core distribution probability  $c_d$  whose value is no greater than its volume fraction  $P^2$ . Each cell in the grid will be assigned a random number by a uniform distribution function within  $(0, 1)$ . Each cell whose random number is no greater than  $c_d$  will be chosen as a core.
- (ii) Expand the core of the growing phase into its neighboring cells in all directions based on its given directional growth probability  $D_i$  where  $i$  represents the

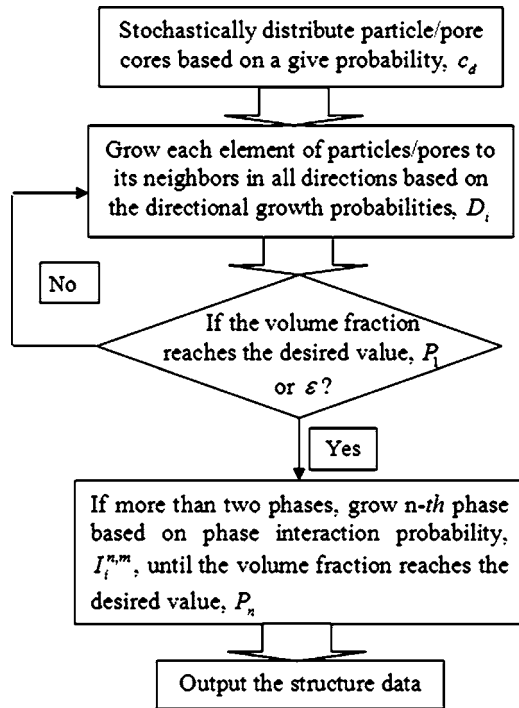


FIG. 2. Flow chart of the QSGS process.

direction. Again new random numbers will be assigned to its neighboring cells; the neighboring cell in direction  $i$  will become part of the growing phase if its random number is no greater than  $D_i$ . Especially for a two-dimensional case, each square elemental cell has eight growing directions to its neighbors, i.e.,  $i = 1, 2, \dots, 8$  as seen in Fig. 3. There are four main directional growth probabilities  $D_{1-4}$  and four diagonal directional growth probabilities  $D_{5-8}$ . To obtain an isotropic structure in such systems, we have to set the directional growth probability ratio  $D_{1-4}:D_{5-8}=4$ , consistent with the equilibrium density distribution function for uniform media.<sup>33</sup>

- (iii) Repeat the growing process of (ii) until the volume fraction of the first growing phase reaches its given value  $P^2$ .
- (iv) As to the next growing phase, there are two cases to

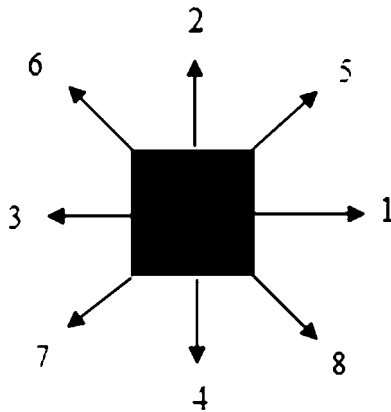


FIG. 3. Eight growth directions of each cell in two-dimensional (2D) systems.

consider depending on its interaction with the existing phase(s). If this phase is an equivalent discrete phase as the existing growing phase, such as a multicomponent mixture, it grows from separate seeds, which is very similar as the first growing phase described in (i)–(iii). Otherwise, we have to consider the constraint by and interaction with the existing phase(s). For such cases, the  $n$ th phase ( $n > 2$ ) will grow based on a phase interaction growth probability  $I_i^{n,m}$ , which represents the growth probability of the  $n$ th phase on the  $m$ th phase along the  $i$ th direction.

- (v) Stop the  $n$ th phase growth once its volume fraction reaches its volume fraction  $P^n$ .
- (vi) Repeat the next phase growth as described in (iv) and (v) until  $n=N$ .
- (vii) The spaces not occupied at the end represent the non-growing phase.

Thus, the four parameters ( $c_d$ ,  $D_i$ ,  $P_n$ , and  $I_i^{n,m}$ ) control the microstructures of generated porous media based on the generation process, whose values can be determined through the statistically analysis of measured data. Comparing with the previous generation methods, this QSGS has the following merits: (i) The generation-growth process is analogous to the natural formation process of some real granular porous media which grow outward from cores. (ii) Each of the parameters in the algorithm has a distinct physical significance, instead of an empirical determination. (iii) It deals well with multicomponent connection problems. (iv) The stochastic and statistical features are introduced smoothly into the system. (v) The method is efficient without turning to any iteration process. Finally the algorithm is straight forward in three-dimensional and/or multiphase cases, and suitable for parallel computing.

## B. Lattice Boltzmann algorithm for electric potential transport equations

The lattice Boltzmann method (LBM) is intrinsically a mesoscopic approach based on the evolution of statistical distribution of lattices, and has achieved considerable success in simulating fluid flows and associated transport phenomena.<sup>52–55</sup> The most important advantages of the LBM are the easy implementations of multiple interparticle interactions and complex geometry boundary conditions,<sup>56</sup> and in general the conservation laws can hold automatically without additional computational efforts.<sup>52,53</sup> The LBM has been developed successfully for simulations of hydrodynamics,<sup>57,58</sup> thermodynamics,<sup>33,34,59</sup> and electrodynamics<sup>60</sup> in porous media. The multiphase conjugate boundary conditions have been developed very recently and it was found that the LBM has a much better efficiency than FDM even for a very simple geometry problem.<sup>61</sup>

For the electric potential transport governing equation [Eq. (1)], we employ the evolution equation on discrete lattices for each phase as

$$g_\alpha(\mathbf{r} + \mathbf{e}_\alpha \delta_t, t + \delta_t) - g_\alpha(\mathbf{r}, t) = -\frac{1}{\tau^n} [g_\alpha(\mathbf{r}, t) - g_\alpha^{\text{eq}}(\mathbf{r}, t)], \quad (9)$$

which is actually a simplified form of the evolution equation for the Poisson equation by eliminating the source terms.<sup>62</sup> The equilibrium distribution of the evolution variable  $g_\alpha$  for the two-dimensional nine-speed (D2Q9) model is

$$g_\alpha^{\text{eq}} = \begin{cases} 0 & \alpha = 0 \\ \frac{1}{6}\Psi & \alpha = 1, 2, 3, 4 \\ \frac{1}{12}\Psi & \alpha = 5, 6, 7, 8, \end{cases} \quad (10)$$

the microscopic velocity is

$$\mathbf{e}_\alpha = \begin{cases} (0, 0) & \alpha = 0 \\ (\cos \theta_\alpha, \sin \theta_\alpha)c & \alpha = 1, 2, 3, 4 \\ \sqrt{2}(\cos \theta_\alpha, \sin \theta_\alpha)c & \alpha = 5, 6, 7, 8, \end{cases} \quad \theta_\alpha = (\alpha - 1)\pi/2 \quad (11)$$

and the dimensionless relaxation time is

$$\tau^n = \frac{3}{2} \frac{\varepsilon_r^n}{c^2 \delta_t} + 0.5, \quad (12)$$

where the subscript  $n$  still represents the  $n$ th phase,  $\delta_t$  is the time step,  $\varepsilon_r$  is the relative dielectric constant, and  $c$  is a pseudo sound speed whose value can theoretically take any positive value to ensure  $\tau$  values within (0.5, 2).<sup>55</sup> The electric potential and flux on each lattice are then calculated by

$$\Psi = \sum_\alpha g_\alpha, \quad (13)$$

$$D = \left( \sum_\alpha \mathbf{e}_\alpha g_\alpha \right) \frac{\tau^n - 0.5}{\tau^n}. \quad (14)$$

For the isopotential boundary treatment, we follow the bounce-back rule of the nonequilibrium distribution proposed by Zou and He.<sup>63</sup> For an insulated boundary, a specular reflection treatment is implemented here to avoid an energy leak along the surfaces.<sup>33</sup> After the potential field is solved, the effective dielectric constant  $\varepsilon_{\text{eff}}$  can then be determined based on Eq. (8) as

$$\varepsilon_{\text{eff}} = \frac{H \int D dL}{\Delta\Psi \int dL}, \quad (15)$$

where  $D$  is the steady electric flux through the cross section area  $dL$  between the electric potential difference  $\Delta\Psi$  with a distance  $H$ .

## IV. RESULTS AND DISCUSSION

We calculate the effective dielectric constant of multiphase microporous media in two steps: reproduce a micro-

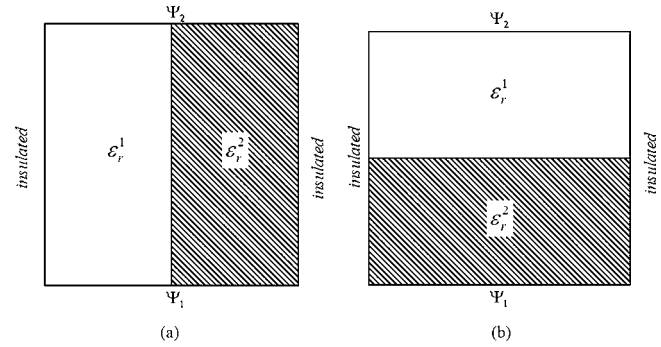


FIG. 4. Two basic structures for validation: (a) parallel mode and (b) series mode.

structure based on its macroscopic geological information using QSGS and then solve the electric potential transport governing equations through the structure by LBM. The effective dielectric property is calculated based on Eqs. (13)–(15). Recently Wang *et al.*<sup>34</sup> have found that the measurement techniques based on a hot probe or a hot wire are actually two-dimensional techniques even though the porous media has three-dimensional structures. Since the hot probe and hot wire are still most popular techniques in measurements of dielectric constant, we present two-dimensional simulations in this contribution. In this section, after the present numerical methods are validated by theoretical solutions for simple structures, they are used to investigate the effects of phase distributions and interactions on the effective dielectric constant of multiphase microporous media. The predictions will be compared with existing experimental data.

### A. Initial validations

First we calculate the effective dielectric constant for two basic structures of double-component materials: the parallel mode and the series mode (see Fig. 4). Assuming the dielectric constants of each component are  $\varepsilon_r^1$  and  $\varepsilon_r^2$ , respectively, the simple theoretical solutions offer the effective dielectric constant as  $(\varepsilon_r^1 + \varepsilon_r^2)/2$  for the parallel mode and  $1/(1/2\varepsilon_r^1 + 1/2\varepsilon_r^2)$  for the series mode.<sup>40</sup>

Table I lists our calculated effective dielectric constant comparing with above theoretical solutions for different values of  $\varepsilon_r^1 : \varepsilon_r^2$ . We keep  $\varepsilon_r^1$  as 1.0 while changing  $\varepsilon_r^2$  from 2.0 to 10 000 using a grid of  $200 \times 200$ . Such a large contrast between  $\varepsilon_r^1$  and  $\varepsilon_r^2$  leads to a long computational time to converge to a steady result, and yet provides a good test on our model. The deviations between the predictions are not greater than 0.006% for the parallel mode and 0.765% for the series mode even in such large dielectric constant contrasts, demonstrating a good accuracy of our approach.

### B. Particle size effect

Several researchers have reported that the effective dielectric constant of porous media may differ from each other for different average pore/particle sizes even though the components and the porosities of the media are the same,<sup>6,7</sup> and yet few analyses have been found to predict these phenomena nicely so far. Here we control the average pore/

TABLE I. Comparisons between predicted results and theoretical solutions with  $\varepsilon_r^1=1.0$ .

$\varepsilon_r^1:\varepsilon_r^2$	Results					
	Parallel mode			Series mode		
	Theoretical value	Present predictions	Relative deviations (%)	Theoretical value	Present predictions	Relative deviations (%)
1:2	1.500	1.500	0.000	1.333	1.332	0.075
1:10	5.500	5.500	0.000	1.818	1.815	0.165
1:100	50.50	50.50	0.000	1.980	1.976	0.202
1:500	250.5	250.5	0.000	1.996	1.991	0.250
1:1000	500.5	500.5	0.000	1.998	1.993	0.250
1:10 000	5000.5	5000.2	0.006	1.9998	2.0151	0.765

particle size by changing the values of the particle core distribution probability  $c_d$  so that a greater value of  $c_d$  leads to a smaller average size of particles for a certain volume fraction.<sup>33</sup> Figure 5 demonstrates two thus generated structures at given solid particle volume fraction  $P^s=0.5$ , where  $c_d$  in Fig. 5(a) is ten times of that in Fig. 5(b). The structure for a higher  $c_d$  looks more uniform and has a higher surface-to-volume ratio.

After the porous structures are generated at different  $c_d$  values, the particle size effect on the effective dielectric constant of porous media is then investigated on a grid of  $200 \times 200$ . Figure 6 shows the predicted effective dielectric constant versus the solid volume fraction  $P^s$  at two different  $c_d$  values. The relative dielectric constants of the components are  $\varepsilon_r^s=5.0$  and  $\varepsilon_r^g=1.0$ , where the superscript  $s$  represents the solid phase and  $g$  the gas phase. The theoretical solutions for the parallel mode and series mode are also compared in the same figure. The results show that the effective dielectric constants of random porous media are between the values of the parallel mode and series mode (the upper and low bounds), and a larger average particle size leads to a lower effective dielectric constant of porous media for all range of porosity except at 0 and 1. The largest difference between the effective dielectric constants at different  $c_d$  values occurs when the solid fraction is within 0.5–0.8. Thus we hold the solid volume fraction  $P^s=0.5$  and change the  $c_d$  value instead. The predicted effective dielectric constants at different values of  $c_d$  are then shown in Fig. 7, indicating that the effective dielectric constant increases with the core distribution probability  $c_d$ . Since the average particle volume is in-

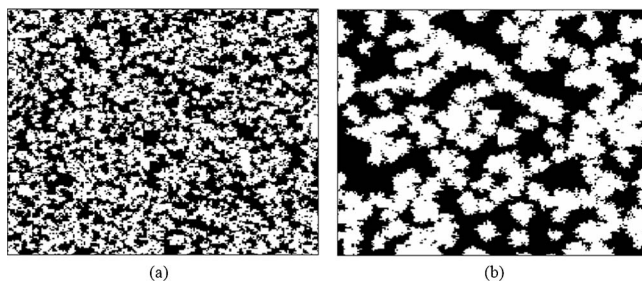


FIG. 5. Structures for different values of  $c_d$  at  $P^s=0.5$ . The directional parameters are set as  $D_{1-4}:D_{5-8}=4:1$ . The dark area is gas and the white the solid. (a)  $c_d=0.1P^s$  and (b)  $c_d=0.01P^s$ .

versely proportional to the value of  $c_d$ , the result suggests the effective dielectric constant of porous media decreases monotonically with the average particle size.

In Fig. 7, we performed three trails for each value of  $c_d$ . The calculated effective dielectric constants do not fall into the same value for each trail, but fluctuated around an averaged value due to the stochastic characteristics of generated structure geometries. The results show that when  $c_d$  is smaller than  $0.005 P^s$  the fluctuations become quite big; while once  $c_d$  is larger than  $0.01 P^s$ , the fluctuations are in a very low level ( $<3\%$ ).

### C. Anisotropy effect

Most previous works have focused on the isotropic cases of porous media. A few researchers have generated an anisotropic porous material by putting groups of ellipses together with different axis lengths or orientation angles.<sup>8</sup> Here we can achieve anisotropic phase distributions easily based on the QSGS process by choosing different values of the directional growth probability  $D_i$ . Figure 8 shows the generated structures for different ratio values of  $D_x:D_y$ , where  $D_x$  are the horizontal main directions (directions 1 and 3 in Fig. 3) and  $D_y$  are the vertical main directions (directions 2 and 4 in Fig. 3). We set  $D_{5-8}=D_y/4$  and the other parameters  $P^s$

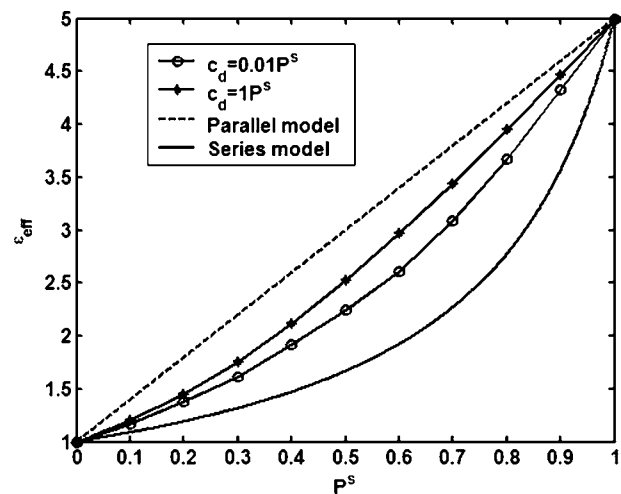


FIG. 6. Effective dielectric constant vs solid volume fraction for different values of  $c_d$ .

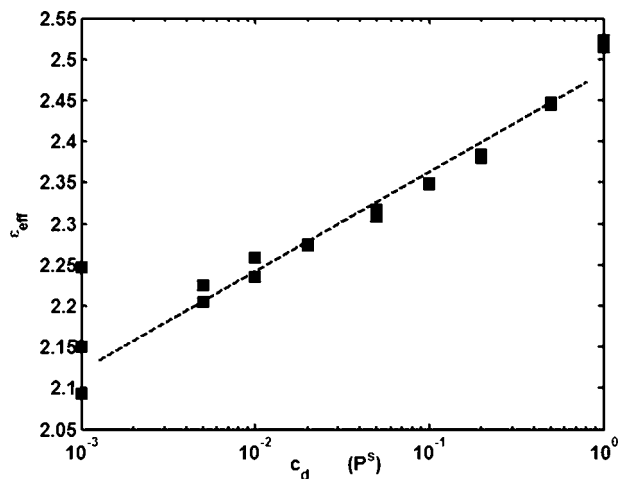


FIG. 7. Effective dielectric constant vs values of  $c_d$  for  $P^s=0.5$ .

$=0.5$  and  $c_d=0.01P^s$ . The grid used is  $200 \times 200$ . The microstructures generated shows quite different characteristics with different values of directional growth probabilities. The anisotropy increases with the  $D_x:D_y$  ratio. The directional growth probability corresponds to the macrostructure statistical orientation features, and can thus be determined by measurement data from real porous structures.

After the anisotropic microstructures are generated, we change the  $D_x:D_y$  ratio from 1/100 to 100 and depict the predicted effective dielectric constant along the vertical direction. Figure 9 shows the numerical results where  $P^s=0.5$ ,  $c_d=0.01P^s$ ,  $\epsilon_r^s=5.0$ , and  $\epsilon_r^g=1.0$ . The results indicate that the effective dielectric constant decreases monotonically with the increasing ratio of  $D_x:D_y$ . For a given porosity, the effective dielectric constant is enhanced along the direction with a higher growth probability and weakened meanwhile along the orthogonal direction.

**D. Phase aggregation effect**

When a porous medium contains more than two phases, the multiphase interaction effects on the material properties have to be considered. For a three-phase porous medium with gas, liquid, and solid, the simplest case is to generate the liquid phase with a uniform phase interaction growth probability, i.e.,  $I_i^l:I_i^s=1$  with  $l$  representing the liquid phase and  $s$  the solid phase. This hypothesis is based on a strong wetting effect caused by a strong liquid-solid attractive potential, and will result in a uniform liquid film at

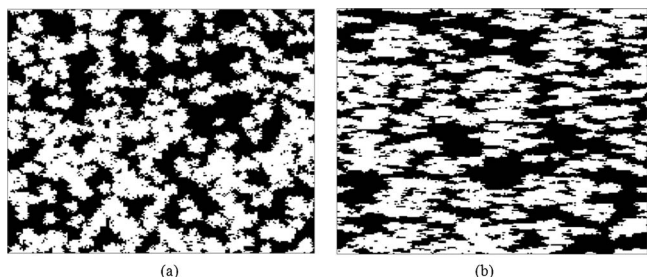


FIG. 8. Microstructures of anisotropic porous media with different directional growth probabilities at  $c_d=0.01P^s$  and  $P^s=0.5$ . The dark is gas and the white is solid. (a)  $D_x:D_y=1:1$  and (b)  $D_x:D_y=10:1$ .

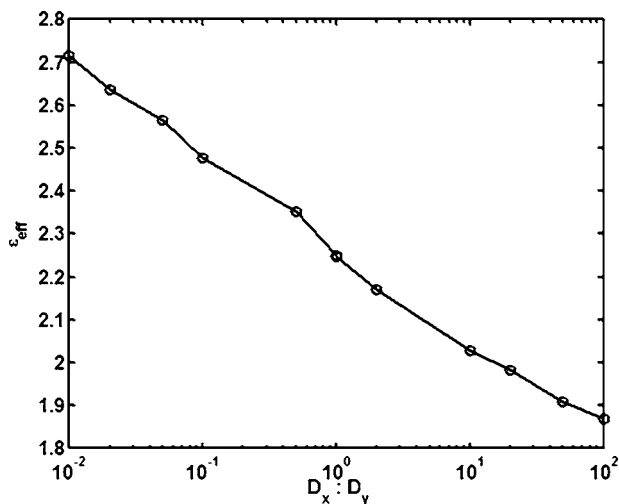


FIG. 9. Effective dielectric constant of anisotropic porous media for different  $D_x:D_y$ .

tached on the solid grains as shown in Fig. 10(a). The smaller is the  $I_i^l:I_i^s$  ratio, the more uniform is the liquid film [see Fig. 10(b)]. Such structures can be found in some multicomponents composite materials.<sup>12</sup> However, for the unsaturated sandstones or glass assemblies, the wetting characteristic of water may be different. The measured images<sup>53</sup> have shown that the water in sandstones or glass assemblies tends to be in conglomeration form rather than in films on the solid surfaces due to the weak wetting properties. Therefore we also reproduce the water distributions similar to those in sandstones or glass assemblies by enlarging the values of  $I_i^l:I_i^s$  ratio, as shown in Figs. 10(c) and 10(d). Now we can use Fig. 10 to compare the water distributions in porous media at different phase interaction growth probabilities. The solid phase distributions are anisotropic with the volume fraction  $P^s=0.5$  and  $c_d=0.01P^s$ . The volume fraction for water  $P^l$  is 0.25 and the ratio of  $I_i^l:I_i^s$  changes from 10:1 to 1:100. A greater  $I_i^l:I_i^s$  ratio corresponds to a weaker wetting interface, i.e., the liquid as a result will be more aggregative.

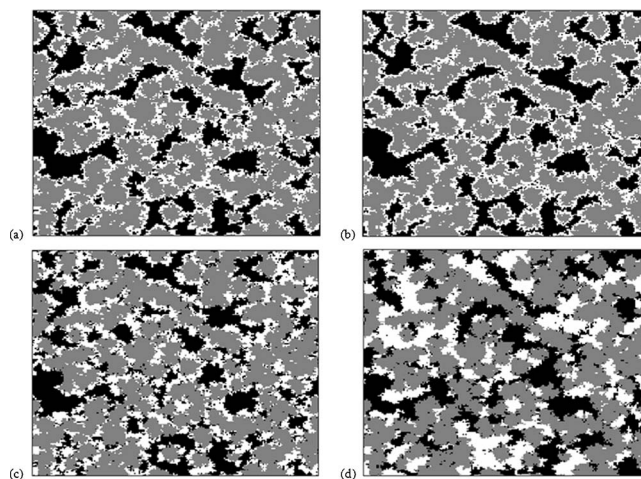


FIG. 10. Microstructures of three-phase porous media with different phase interaction growth probabilities. The gray is the solid particles, the white is the liquid, and the dark is the gas. The solid phase is isotropic with  $P^s=0.5$  and  $c_d=0.01P^s$ , and the liquid volume fraction with  $P^l=0.25$ . (a)  $I_i^l:I_i^s=1:1$ , (b)  $I_i^l:I_i^s=1:10$ , (c)  $I_i^l:I_i^s=10:1$ , and (d)  $I_i^l:I_i^s=100:1$ .

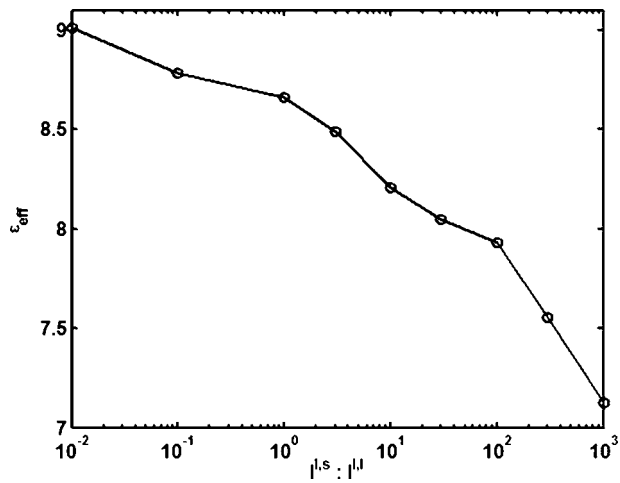


FIG. 11. Effective dielectric constants of three-phase porous media for different liquid-solid phase interaction growth probabilities.

The influences of the phase interaction growth probability on the effective dielectric constant of multiphase porous media are better illustrated in Fig. 11. Assuming again the unsaturated sandstone case where the solid particle volume fraction is  $P^s=0.5$  and  $c_d=0.01P^s$ , the water volume fraction is  $P^l=0.3$ , and the dielectric constants of each phase are  $\epsilon_r^s=5.0$ ,  $\epsilon_r^l=80$  and  $\epsilon_r^g=1.0$ , respectively. Figure 11 shows the predicted effective dielectric constants at different liquid-solid phase interaction growth probabilities. The present results indicate that the effective dielectric constant of multiphase porous media decreases with the ratio  $I_i^l:I_i^s$  and has a more drastic reduction at a higher  $I_i^l:I_i^s$  ratio, or for a weaker wetting interface.

### E. Comparisons with experimental data

Finally, our predictions are compared quantitatively with some published data of the measured dielectric constant of multiphase porous media as well. As there is little information presented along with the experimental data in those studies, we are not able to assign the geometrical parameters for the QSGS model with certainty and have to evaluate their values from related information. For simplification, we suppose the porous structures in the comparison are isotropic ( $D_{1-4}:D_{5-8}=4:1$ ), and the solid surface is hydrophilic ( $I_i^l:I_i^s=1$ ) in case of three-phase systems. The two assumptions, especially the latter one, may not be true to the original experiments and may thus lead to deviations in our predictions, and more strict validations can be done if both geometry information and measured dielectric properties are available.

Consider a glass porous structure that is either dry or saturated fully by a liquid, i.e., a two-phase case. Sen *et al.* measured the dielectric constant of such porous systems in three cases: dry, water saturated and methanol saturated.<sup>64</sup> We reproduce porous structures by QSGS with  $c_d=0.01P^{\text{glass}}$  on  $200 \times 200$  grids and calculate the effective dielectric constant by LBM with the component dielectric properties:  $\epsilon_r^{\text{water}}=80$ ,  $\epsilon_r^{\text{methanol}}=30$ ,  $\epsilon_r^{\text{air}}=1$ , and  $\epsilon_r^{\text{glass}}=6.4$ .<sup>64</sup> Figure 12 shows the predicted effective dielectric constant versus the porosity ( $1-P^{\text{glass}}$ ) for the three cases compared

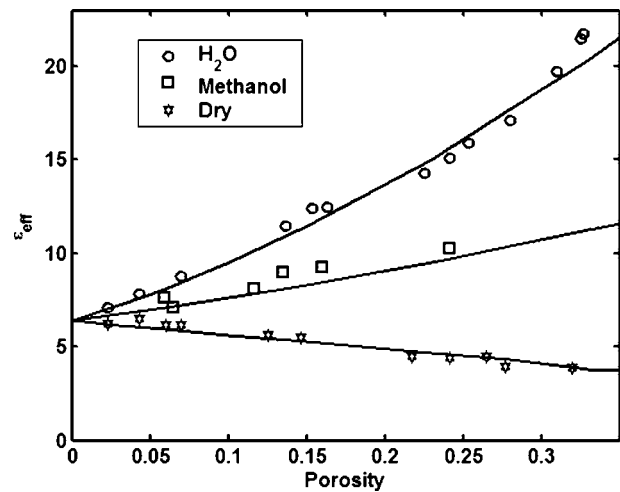


FIG. 12. Effective dielectric constant vs porosity for porous glass (two-phase cases) where  $c_d=0.01P^{\text{glass}}$ ,  $\epsilon_r^{\text{water}}=80$ ,  $\epsilon_r^{\text{methanol}}=30$ ,  $\epsilon_r^{\text{air}}=1$ , and  $\epsilon_r^{\text{glass}}=6.4$ .

with the experimental data. The symbols are the experimental data<sup>64</sup> and the solid lines are the predicted values. The numerical results show good agreements with the experimental data.

When the solid porous structure is partially saturated by the liquid, the effective dielectric constant of the multiphase system may change greatly with the liquid content. A technique has been developed by that the volumetric water content can be evaluated from the measured value of effective dielectric constant of unsaturated soil sample.<sup>7,9,16,22</sup> Here we simulate such a three-phase system using the present numerical methods. Figure 13 compares our predicted effective dielectric constant of such unsaturated soil with the measured data of Andisoil (Miyamoto *et al.*) (Ref. 65) and those by other theoretical models reported in Refs. 16 and 66. The solid soil particles are reproduced by QSGS with  $P^{\text{soil}}=0.27$  and  $c_d=0.01P^{\text{soil}}$ . The component dielectric properties used are  $\epsilon_r^{\text{water}}=80$ ,  $\epsilon_r^{\text{soil}}=5.5$ , and  $\epsilon_r^{\text{air}}=1$ .<sup>66</sup> Comparing with the results by other theoretical models, the present predictions agree most closely with the experimental data. The

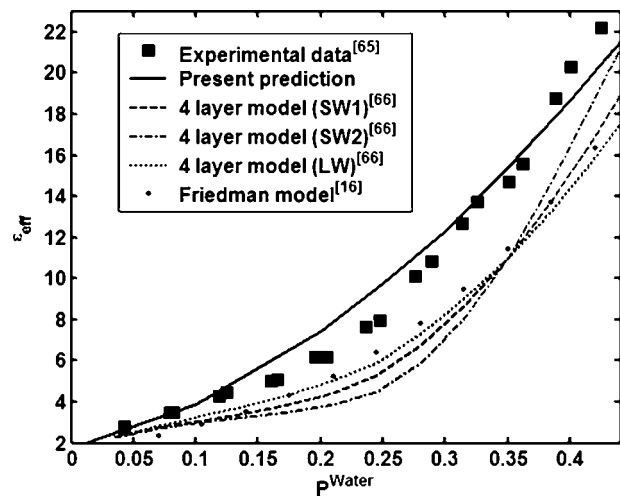


FIG. 13. Effective dielectric constant vs volumetric water content for unsaturated soil (three-phase cases) where  $\epsilon_r^{\text{water}}=80$ ,  $\epsilon_r^{\text{soil}}=5.5$ , and  $\epsilon_r^{\text{air}}=1$ .

agreements should be better if we know the geometry accurately so as to use more correct geometrical parameters in QSGS.

## V. CONCLUSIONS

This paper provides a full numerical tool set for modeling and predicting a frequency-independent effective dielectric constant of multiphase microporous media, including a multiparameter random generation-growth algorithm for generating microstructures of multiphase porous media, and a lattice Boltzmann solver for the electric potential transport equations on porous structures. After validated by the theoretical solutions for simple geometries, the present methods are used to investigate the phase distribution effects on the effective dielectric constant of multiphase microporous media, such as the particle size effect, anisotropy effect, and phase aggregation effect for different wetting characteristics between phases. The results show that a smaller average particle size leads to a larger effective dielectric constant at given porosity; the effective dielectric constant will be enhanced along the relatively larger directional growth probability, which controls the anisotropy of the generated porous media, and as a result the effective dielectric constant in the other direction is weakened. For multiphase porous media, the degree of phase aggregation is determined by the surface wetting properties and controllable by the phase interaction growth probabilities in our model, and simulations for unsaturated soil show that the effective dielectric constant of three-phase porous media decreases with the degree of liquid phase aggregation. The present predictions agree well with the existing experimental data for both two-phase and three-phase cases.

## ACKNOWLEDGMENTS

The present work is supported by a grant from the NTC-M04-CD01. The authors would like to thank Dr. Miyamoto for providing the experimental data.

- <sup>1</sup>G. K. Batchelor, *Annu. Rev. Fluid Mech.* **6**, 227 (1974).
- <sup>2</sup>D. K. Hale, *J. Mater. Sci.* **11**, 2105 (1976).
- <sup>3</sup>R. Landauer, in *Electrical Transport and Optical Properties of Inhomogeneous Media*, edited by J. C. Garland and D. B. Tanner (AIP, New York) Vol. 40, pp. 2–43.
- <sup>4</sup>F. Lux, *J. Mater. Sci.* **28**, 285 (1993).
- <sup>5</sup>S. O. Gladkov, *Dielectric Properties of Porous Media* Springer New York, (2003).
- <sup>6</sup>S. B. Jones and S. P. Friedman, *Water Resour. Res.* **36**, 2821 (2000).
- <sup>7</sup>J. M. Blonquist, S. B. Jones, I. Lebron, and D. A. Robinson, *Water Resour. Res.* **42**, W05424 (2006).
- <sup>8</sup>T. Jonckheere and J. M. Luck, *J. Phys. A* **31**, 3687 (1998).
- <sup>9</sup>M. Persson, B. Sivakumar, R. Berndtsson, O. H. Jacobsen, and P. Schjoning, *Soil Sci. Soc. Am. J.* **66**, 1424 (2002).
- <sup>10</sup>S. D. Logsdon, *Soil Sci. Soc. Am. J.* **69**, 983 (2005).
- <sup>11</sup>C. R. Bowen and D. P. Almond, *Mater. Sci. Technol.* **22**, 719 (2006).
- <sup>12</sup>T. Yamada, T. Ueda, and T. Kitayama, *J. Appl. Phys.* **53**, 4328 (1982).
- <sup>13</sup>L. C. Shen, C. Liu, J. Korringa, and K. J. Dunn, *J. Appl. Phys.* **67**, 7071 (1990).
- <sup>14</sup>B. Sareni, L. Krahenbuhl, and C. Brosseau, *J. Appl. Phys.* **80**, 1688 (1996).
- <sup>15</sup>B. Sareni, L. Krahenbuhl, A. Beroual, and C. Brosseau, *J. Appl. Phys.* **81**, 2375 (1997).
- <sup>16</sup>S. P. Friedman, *Water Resour. Res.* **34**, 2949 (1998).
- <sup>17</sup>D. A. Robinson and S. P. Friedman, *Water Resour. Res.* **37**, 33 (2001).
- <sup>18</sup>S. P. Friedman and D. A. Robinson, *Water Resour. Res.* **38**, 1236 (2002).
- <sup>19</sup>L. Gao and J. Z. Gu, *J. Phys. D* **35**, 267 (2002).
- <sup>20</sup>S. B. Jones and D. Or, *Physica B* **338**, 284 (2003).
- <sup>21</sup>C. Delerue and G. Allan, *Appl. Phys. Lett.* **88**, 173117 (2006).
- <sup>22</sup>S. P. Friedman, *Comput. Electron. Agric.* **46**, 45 (2005).
- <sup>23</sup>S. Torquato, I. C. Kim, and D. Cule, *J. Appl. Phys.* **85**, 1560 (1999).
- <sup>24</sup>H. F. Zhang, X. S. Ge, and H. Ye, *J. Phys. D* **39**, 220 (2006).
- <sup>25</sup>L. Tacher, P. Perrochet, and A. Parriaux, *Transp. Porous Media* **26**, 99 (1997).
- <sup>26</sup>M. Pilotti, *Transp. Porous Media* **33**, 257 (1998).
- <sup>27</sup>K. Makrodimitris, G. K. Papadopoulos, C. Philippopoulos, and D. N. Theodorou, *J. Chem. Phys.* **117**, 5876 (2002).
- <sup>28</sup>D. S. Li, G. Saheli, M. Khaleel, and H. Garmestani, *Comput. Mater. Sci.* (in press).
- <sup>29</sup>N. Losic, J. F. Thovert, and P. M. Adler, *J. Colloid Interface Sci.* **186**, 420 (1997).
- <sup>30</sup>S. Torquato, *Random Heterogeneous Materials: Microstructure and Macroscopic Properties* (Springer, New York, (2002).
- <sup>31</sup>S. Torquato, *Int. J. Solids Struct.* **37**, 411 (2000).
- <sup>32</sup>S. Mohanty, *J. Phys. D* **30**, L80 (1997).
- <sup>33</sup>M. Wang, J. K. Wang, N. Pan, and S. Chen, *Phys. Rev. E* **75**, 036702 (2007).
- <sup>34</sup>M. Wang, J. K. Wang, N. Pan, S. Chen, and J. He, *J. Phys. D* **40**, 260 (2007).
- <sup>35</sup>P. Meakin, *Fractals, Scaling and Growth far from Equilibrium* (Cambridge University Press, Cambridge 1998).
- <sup>36</sup>K. Karkkainen, A. Sihvola, and K. Nikoskinen, *IEEE Trans. Geosci. Remote Sens.* **39**, 1013 (2001).
- <sup>37</sup>K. Asami, *J. Colloid Interface Sci.* **292**, 228 (2005).
- <sup>38</sup>K. Asami, *J. Phys. D* **39**, 492 (2006).
- <sup>39</sup>J. P. Calame, *J. Appl. Phys.* **99**, 084101 (2006).
- <sup>40</sup>E. Tuncer and S. M. Gubanski, *J. Appl. Phys.* **89**, 8092 (2001).
- <sup>41</sup>I. Krakovsky and V. Myroshnychenko, *J. Appl. Phys.* **92**, 6743 (2002).
- <sup>42</sup>A. Myroshnychenko and C. Brosseau, *Phys. Rev. E* **71**, 016701 (2005).
- <sup>43</sup>A. Mejdoubi and C. Brosseau, *J. Appl. Phys.* **100**, 094103 (2006).
- <sup>44</sup>K. Sekine, C. Kuroda, and N. Torii, *Colloid Polym. Sci.* **280**, 71 (2002).
- <sup>45</sup>K. Sekine, Y. Watanabe, S. Hara, and K. Asami, *Biochim. Biophys. Acta* **1721**, 130 (2005).
- <sup>46</sup>D. X. Zhang, *Stochastic Method for Flow in Porous Media* Academic Press, London, (2002).
- <sup>47</sup>D. B. Ingham and I. Pop, *Transport Phenomena in Porous Media III*, (Elsevier, Oxford, UK, 2005).
- <sup>48</sup>W. Z. Yue, G. Tao, and K. Q. Zhu, *Chin. J. Geophys.-Chin. Ed.* **47**, 905 (2004).
- <sup>49</sup>W. Z. Yue, G. Tao, and K. Q. Zhu, *Chin. J. Geophys.-Chin. Ed.* **48**, 189 (2005).
- <sup>50</sup>C. Y. Chan and R. J. Knight, *Water Resour. Res.* **37**, 1099 (2001).
- <sup>51</sup>S. Moysey and R. Knight, *Water Resour. Res.* **40**, W03510 (2004).
- <sup>52</sup>S. Y. Chen and G. D. Doolen, *Annu. Rev. Fluid Mech.* **30**, 329 (1998).
- <sup>53</sup>S. Succi, *The Lattice Boltzmann Equation for Fluid Dynamics and Beyond* (Oxford Science Press, London, (2001).
- <sup>54</sup>D. Raabe, *Modell. Simul. Mater. Sci. Eng.* **12**, R13 (2004).
- <sup>55</sup>J. K. Wang, M. Wang, and Z. X. Li, *J. Colloid Interface Sci.* **296**, 729 (2006); M. Wang, J. K. Wang, and Z. X. Li, *J. Colloid Interface Sci.* **300**, 446 (2006).
- <sup>56</sup>Q. J. Kang, D. X. Zhang, P. C. Lichtner, and I. N. Tsimpanogiannis, *Geophys. Res. Lett.* **31**, L21604 (2004).
- <sup>57</sup>Q. J. Kang, D. X. Zhang, and S. Y. Chen, *J. Geophys. Res.* **108**, 2505 (2003).
- <sup>58</sup>Q. J. Kang, D. X. Zhang, and S. Y. Chen, *Phys. Rev. E* **66**, 056307 (2002).
- <sup>59</sup>M. Wang, J. H. He, J. Y. Yu, and N. Pan, *Int. J. Therm. Sci.* (10.1016/j.ijthermalsci.2006.11.006).
- <sup>60</sup>M. Wang, J. K. Wang, S. Chen, and N. Pan, *J. Colloid Interface Sci.* **304**, 246 (2006).
- <sup>61</sup>J. K. Wang, M. Wang, and Z. X. Li, *Int. J. Therm. Sci.* **46**, 228 (2007).
- <sup>62</sup>J. K. Wang, M. Wang, and Z. X. Li, *Commun. Nonlinear Sci. Numer. Simul.*
- <sup>63</sup>Q. S. Zou and X. Y. He, *Phys. Fluids* **9**, 1591 (1997).
- <sup>64</sup>P. N. Sen, C. Scala, and M. H. Cohen, *Geophysics* **46**, 781 (1981).
- <sup>65</sup>T. Miyamoto, T. Annaka, and J. Chikushi, *Vadose Zone J.* **2**, 90 (2003).
- <sup>66</sup>T. Miyamoto, T. Annaka, and J. Chikushi, *Soil Sci. Soc. Am. J.* **69**, 23 (2005).